A Local Nonlinear System Model of the Turbulent Boundary Layer

S. Midya

Institute for Flow Physics and Control
University of Notre Dame
Notre Dame, Indiana-46556
midya.1@nd.edu

F. O. Thomas

Institute for Flow Physics and Control
University of Notre Dame
Notre Dame, Indiana-46556
fthomas@nd.edu

T. C. Corke

Institute for Flow Physics and Control
University of Notre Dame
Notre Dame, Indiana-46556
tcorke@nd.edu

ABSTRACT

The interaction between the near-wall and logarithmic layer in a high Reynolds number zero pressure gradient turbulent boundary layer is examined in terms of polyspectal measurements. The near wall velocity fluctuation skewness is decomposed in frequency space via the real part of the autobispectrum. Similarly, the cross-bicoherence is used to examine the nonlinear phase coupling between the near wall region and logarithmic layer. These measurements clearly show the importance of quadratically nonlinear mechanisms in characterizing the near wall-outer layer interaction. To this end, a Volterra nonlinear system model containing both linear and quadratically nonlinear system transfer functions is proposed to model the near-wall outer layer interaction, It is demonstrated that the transfer functions may be determined via measured polyspectal quantities and the system output due to linear, quadratic and linear-quadratic coupling mechanisms quantifield.

INTRODUCTION

It is now widely accepted that large-scale vortical structures are an important and universal feature of the outer region of wall bounded turbulent flows (e.g. Hutchins and Marusic (2007), Adrian (2007), Monty et al (2007), Marusic et al (2010), Smits, McKeon and Marusic (2011) and others). It has also been demonstrated that these outer layer structures impose their imprint on the near-wall region of the turbulent boundary layer in the form of the amplitude and phase modulation of near-wall velocity and wall shear stress fluctuations (e.g. Hutchins and Marusic (2007), Mathis et al (2009), Ganipathisubramani et al (2009)). In addition, Mathis et al (2011) demonstrate that the skewness of velocity fluctuations in the near-wall region is directly linked to amplitude modulation.

The nature of the interation between outer and inner regions of wall bounded flows is of both fundamental and practical interest since the near-wall region is responsible for turbulence production. Schoppa and Hussain (2002) described a streak transient growth (STG) mechanism for the self-sustaining mechanism of near-wall turbulence generation. They suggested that STG was the dominant streamwise vortex generation mechanism from otherwise normal mode stable low-speed streaks. In related work, Schoppa and Hussain (1998) proposed a large-scale strategy for skin friction drag reduction which was demonstrated in channel flow DNS. By imposing a streamwise-independent, spanwise velocity component along the channel wall by means of either a pair of counter-rotating streamwise vortices, or opposed wall jets significant drag reduction was achieved. The flow control served to prevent the lift-up of low-speed streaks, thereby limiting their flanking wall-normal vorticity component which in their formulation, is a critical parameter for onset of STG. More recently, their channel flow drag reduction work was revisited by Canton et al (2016), where comparable levels of sustained drag reduction were achieved by a volumetric forcing approach. Motivated by this work a novel, nonintrusive, flush surface-mounted pulsed-DC plasma actuator was recently designed at the University of Notre Dame to be the first to actively intervene in the STG mechanism by producing a near-wall spanwise flow component that prevents the lift-up of low-speed streaks. Experiments show the abiliy of the actuator to very significnatly decrease or increase drag depending on the magnitude of the imposed spanwise velocity (Thomas et al (2016)).

Aside from the practical aspects pertaining to drag reduction, the pulsed-DC actuator also provides an experimental tool by which the nature of the outer region-inner layer interaction can be investigated under both reduced and enhanced drag conditions and compared to the natural flow. Furthermore, in order to characterize the dynamic interaction between the near-wall and outer regions of the TBL a second-order Volterra nonlinear system model is applied. This model involves the determination of both linear and nonlinear system transfer functions that characterize the interaction. A particular focus of this paper is to describe and motivate the application of the nonlinear sytem model to the turbulent boundary layer.

EXPERIMENTAL FACILITY

The turbulent boundary layer measurements were conducted in a large in-draft wind tunnel facility located at the University of Notre Dame with a test section cross sectional area of 1.5 m ×1.5 m, a working test section length of 15.25m, and a maximum speed of approximately 13.5m/s. The inlet is 3.05 m × 3.05 m and corresponds to a contraction ratio of 4:1. A screen box is placed behind the inlet consisting of 4 stainless steel turbulence reduction screens (mesh spacing = 1 mm and wire diameter = 0.1 mm) with

0.229 m streamwise spacing between individual screens and 0.204 m thick honeycomb (0.013 m diameter) placed directly upstream of the screens. The resulting free stream turbulence intensity measured 9.14 m downstream of the inlet was $\sqrt{\overline{u^2}}/U_\infty \leq 0.5$ %. The wind tunnel is constructed of 1.9 cm plywood and also has a plexiglass side-wall for full optical access. In order to reduce surface roughness, a subfloor made of pressed particle board was installed over the plywood. Two essential characteristics of the experimental facility are that it must provide a ZPG turbulent boundary with (1) very high Re_τ ($\equiv \frac{U_\tau \delta}{\nu}$) and (2) large boundary layer thickness thereby allowing measurements of high wall-normal spatial resolution. Although the experiments are performed in a low-speed tunnel, its large streamwise fetch allows high Reynolds numbers to be achieved (Re_x as large as 9 x 10^6). This facility has been used to acquire ZPG turbulent boundary layer measurements at $Re_\tau \approx 3200$. Representative samples of these data are presented in the next section.

TURBULENT BOUNDARY LAYER CHARACTERISTICS

Figure 1a presents a sample turbulent boundary layer mean velocity profile obtained at the streamwise location of x = 12.2 m which corresponds to $Re_\tau \approx 3200$. The profile is presented using inner variable scaling with the Clauser method used to obtain the local friction velocity. The mean velocity profile is observed to exhibit a well-defined logarithmic region for $30 \leq y^+ \leq 700$ in excellent agreement with classic log law of the wall. Figure 1b presents the corresponding streamwise component turbulence intensity profile using inner variable scaling. Consistent with previous studies, the profile exhibits a near-wall peak value of $\frac{\overline{u^2}}{U_\tau^2} = 7.25$ at $y^+ \approx 15$. There is also indication of a weaker peak in the logarithmic region centered near $y^+ \approx 250$.

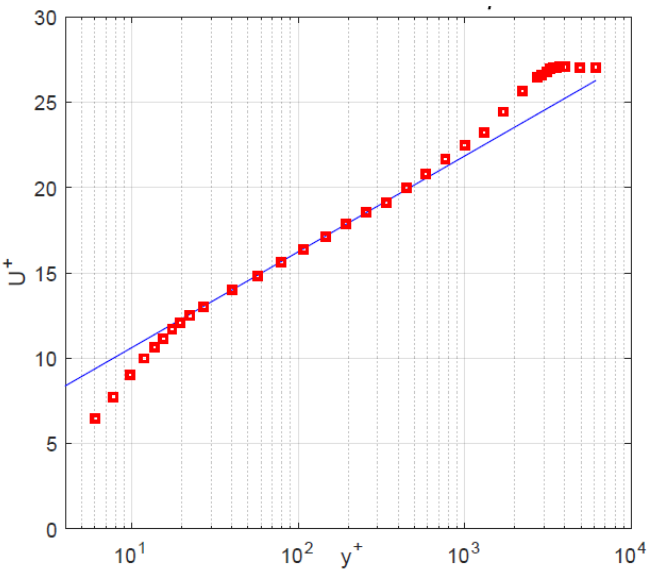

Figure 1a. Mean velocity profile ($Re_\tau \approx 3200$).

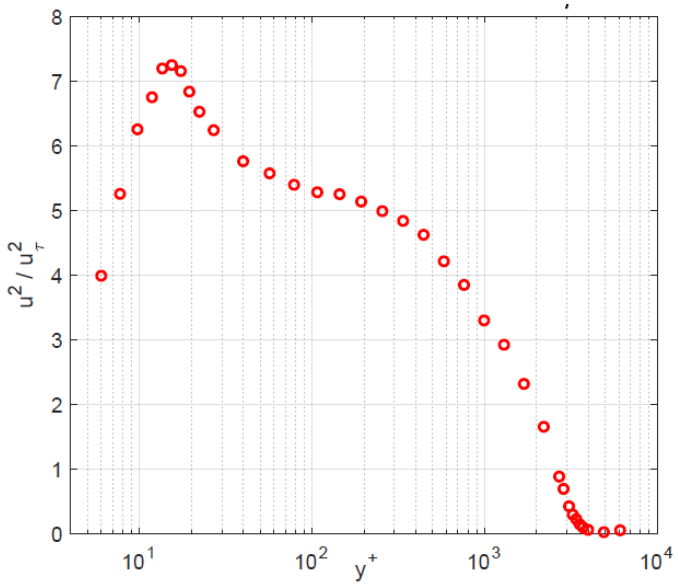

Figure 1b. Streamwise component turbulence intensity profile ($Re_\tau \approx 3200$).

Figure 2 presents the skewness factor profile, $S_u = \overline{u^3}/(\overline{u^2})^{3/2}$, as a function of y^+. This result is also in very good agreement with previous measurements in high-Reynolds number turbulent boundary layers. In particular, S_u is positive in the near-wall region ($y^+ \leq 20$) and becomes negative for $y^+ \geq 130$. Note that the large-values of the skewness factor near the edge of the boundary layer are heavily influenced by intermittency associated with the turbulent / non-turbulent interface.

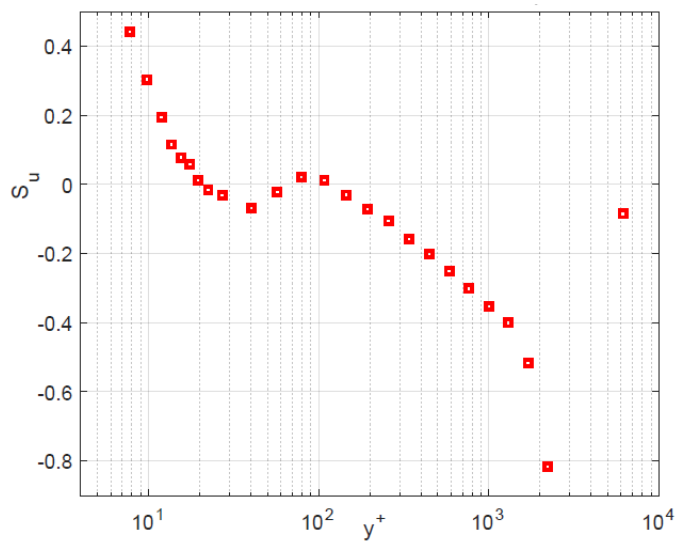

Figure 2. TBL skewness factor profile ($Re_\tau \approx 3200$).

The spectral content of the ZPG turbulent boundary layer in streamwise component wavenumber domain was examined in terms of the pre-multiplied 1-D auto spectral density of the streamwise component fluctuation, $k_x \phi_{uu}/U_\tau^2$. This is presented in Figure 3a as a function of both $y^+$and inner-variable scaled streamwise wave number, λ_x^+. The assumed convective speed to

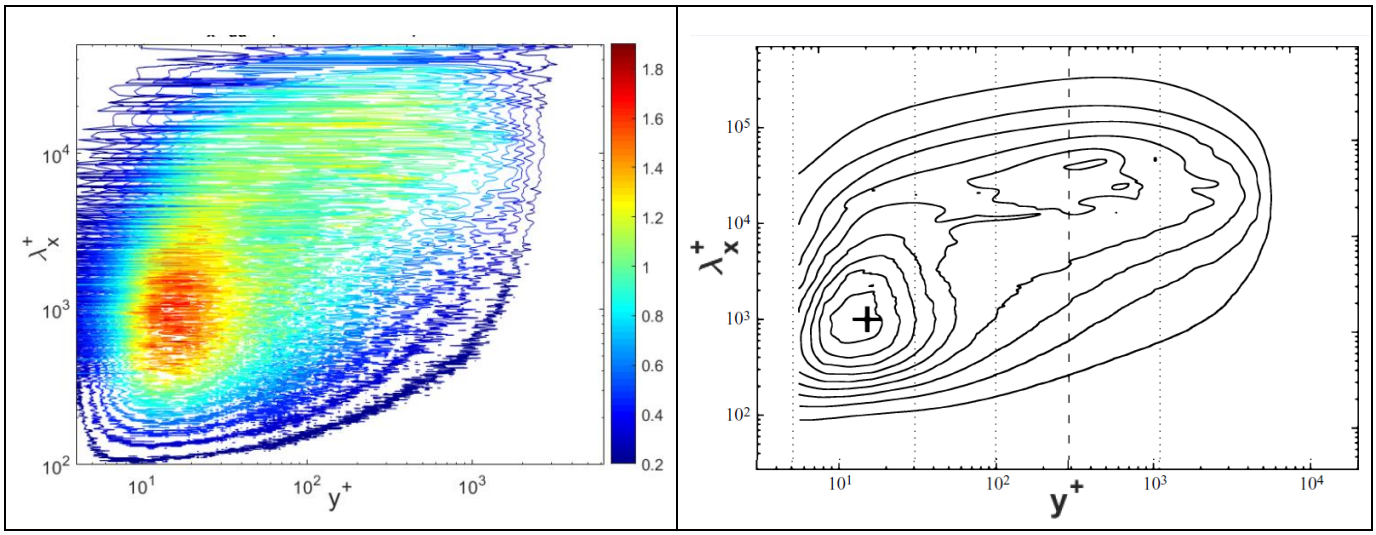

Figure 3 (a) Contours of pre-multiplied energy 1-D wavenumber spectra obtained in the Notre Dame facility at $Re_\tau \approx 3200$. (b) Contours of pre-multiplied energy 1-D wavenumber spectra obtained by Mathis et al (JFM, 2009) at $Re_\tau \approx 7300$.

convert to 1-D wavenumber domain was the local mean speed. The pre-multiplied energy spectra of the streamwise velocity fluctuation shows an inner peak located at $y^+ = 15$ and centered at $\lambda_x^+ = 1000$. A weaker outer peak appears near $y^+ \approx 250$, $y/\delta \approx 0.06$ with a much larger wavelength $\lambda_x^+ \approx 20000$, $\lambda_x/\delta \approx 5$. Figure 3b shows comparable ZPG turbulent boundary layer pre-multiplied energy wavenumber spectra as obtained by Mathis et al (2009). The inner and outer spectral peaks noted in Figure 3a are also apparent in this case. In fact, the outer peak is more apparent in Figure 3b and this is likely a consequence of the higher Re_τ of the Mathis et al (2009) experiment, $Re_\tau \approx 7300$.

NATURE OF NEAR-WALL AMPLITUDE MODULATION

As previously noted, small-scale velocity fluctuations in the near-wall region of the turbulent boundary layer undergo amplitude and phase modulation by larger-scales structures in the outer region. The correlation between near-wall amplitude modulation and large-scale structure in the boundary layer has been quantified in terms of an amplitude modulation correlation coefficient, R, which was defined by Mathis et al (2009) as,

$$R = \frac{\overline{u_L^+ \, E_L(u_S^+)}}{\sqrt{\overline{u_L^{+2}}}\sqrt{\overline{E_L(u_S^+)^2}}} \qquad (1)$$

Here, u_L^+ and u_S^+ denote the inner-variable scaled large-scale and small-scale velocity fluctuations, respectively. $E_L(.)$ represents the envelope function of the near-wall fluctuations obtained using the Hilbert transform. In this experiment the velocity signal was divided into large and scall-scale parts by using a cutoff frequency of 50 Hz which corresponds to one large eddy turnover timescale (δ/U_∞). Figure 4 presents the measured amplitude modulation correlation coefficient profile. It is found to be in remarkable agreement with R as measured by Mathis et al (2011) at similar Reynolds number. One can also note the striking similarity between the R and S_u profiles shown in Figs 4 and 2 respectively. In forming a scale-decomposed skewness, Mathis et al, 2011 showed that a constituent part of the skewness, $\overline{\overline{3u_L^+ u_S^{+2}}}$ (where $\bar{\bar{X}} = \bar{X}/(\overline{u^2})^{\frac{3}{2}}$), has a profile shape similar to R which is perhaps not surprising since the quantity $\overline{\overline{3u_L^+ u_S^{+2}}}$ actually calculates the correlation between u_L^+ i.e. the large scales and u_S^{+2}, a representative of the envelope of the small scales.

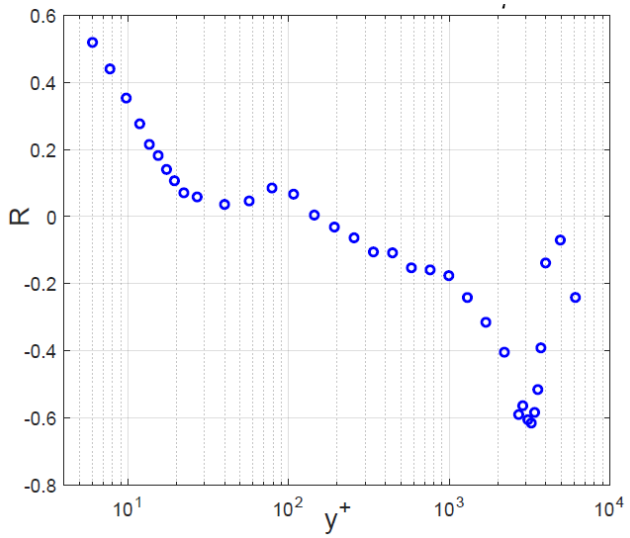

Figure 4: Profile of amplitude modulation coefficient ($Re_\tau \approx 3200$)

Since the amplitude modulation of the near wall fluctuations by structures in the outer region contributes significantly to skewness, it is also of interest to examine the spectral decomposition of the skewness of the near-wall signal. Similar to the spectral decomposition of $\overline{u^2}$ via the autospecral density one can also decompose the skewness in frequency domain using the higher order spectral estimate known as the bispectrum. The bispectrum is defined as,

$$B_{xxx}(f_1^*, f_2^*) = E\,[X_{f^*}^C\, X_{f_1^*} X_{f_2^*}] \quad \text{where} \quad f^* = f_1^* + f_2^* \qquad (2)$$

where $E[.]$ denotes an expected value, X_{f^*} a Fourier transform and the superscript C a complex conjugate. The frequencies have been normalized by the large eddy frequency $f_i^* = f_i \delta / U_\infty$. It is straightforward to show that the real part of the bispectrum is related to the skewness by,

$$E[u^3(t)] = Re(\sum_{f_1^*, f_2^*} B_{xxx}(f_1^*, f_2^*)) \qquad (3)$$

The real part of the bispectrum provides the contribution to the skewness from spectral components f_1^* and f_2^*. The decomposition of the skewness in frequency domain via (3) can reveal information regarding the modes undergoing non linear interaction thereby providing a new persepctive on the nature of the near wall modulation.

Spectral Decomposition of Skewness.

Due to symmetry properties, the bispectrum maps to f_1^* and f_2^* frequency domain shown in Figure 5.

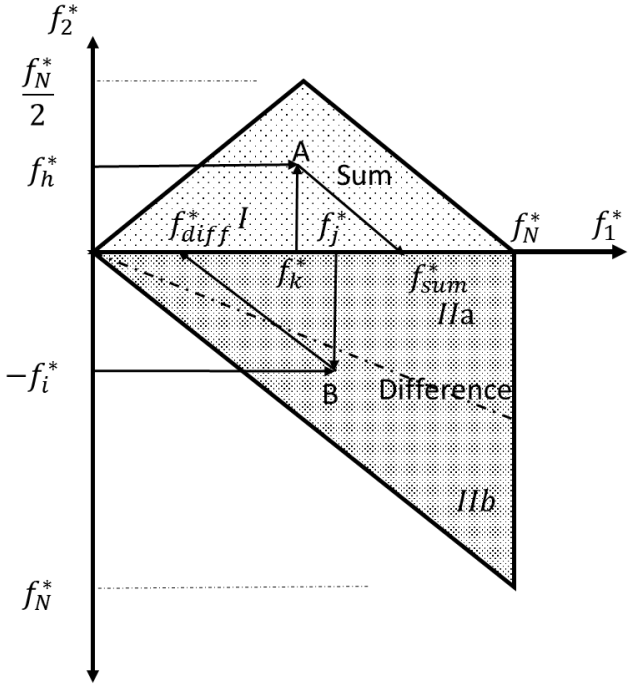

Figure 5: Region of computation for cross bispectrum. The sum and difference interaction regions are also shown.

The upper triangular Region I is associated with triad sum interactions. For example point A is associated with the interaction $f_h^* + f_k^* = f_{sum}^*$. In contrast, Region II is associated with difference interactions. For example, point B corresponds to the difference interaction $f_j^* - f_i^* = f_{diff}^*$. Interactions in region IIb result in difference modes at a freqeuncy less than the intereactimg modes. Interactions in region IIa results in difference modes at an intermediate frequency.

Figure 6 presents iso-contours of the real part of the bisepctrum obtained in the near-wall region at $y^+ = 15$. The real part of the bispectrum shows contours in regions I, IIa and IIb. In Region I, sum interactions are indicated for a range of frequencies up to $f_1^* \leq 8$ with much lower frequencies $f_2^* \leq 0.5$ with many peaks occuring near $f_2^* \leq 0.25$. These interactions are all of form $f_1^* + f_2^* = f_1^* + \delta f^*$ where $\delta f^* \approx O\,(0.25)$. In region IIa a series of difference interactions are indicated between modes $f_1^* \leq 8$ and $f_2^* \geq -0.5$. These are all of form $f_1^* - f_2^* = f_1^* - \delta f^*$ where again $\delta f^* \approx O\,(0.25)$. Finally, in region IIb multiple difference interactions are observed between modes and are of form $f_1^* - f_2^* = f_1^* - (f_1^* - \delta f^*) = \delta f^*$.

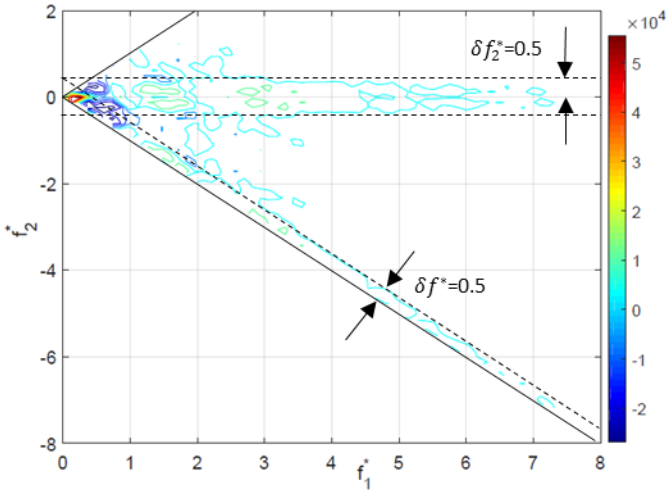

Figure 6. Real part of the bispectrum of the signal of the location $y^+ = 15$. The values are not normalized.

The spectral distribution of skewness reveals mutiple quadratic mode interactions that are local in frequency space in the sense that they involve neighboring Fourier modes whose difference in frequency $\delta f^* \approx O\,(0.25)$ and this likely is associated with the imprint of large-scale motions in the outer layer.

Cross-Bicoherence Measurements

In order to gain further insight regarding the nature of scale interactions between the outer and near wall regions two point cross-bisectral measurements were made. The cross-bispectrum between two signals x(t) and y(t) is given by

$$B_{xxy}(f_1^*, f_2^*) = E[Y_{f^*}^C\, X_{f_1^*} X_{f_2^*}] \quad \text{where} \quad f^* = f_1^* + f_2^* \qquad (4)$$

X_f and Y_f denote the Fourier transforms of x(t) and y(t), respectively. The cross-bicoherence is the normalized version of the cross-bispectrum and is given by,

$$b_{xxy}^2(f_1, f_2) = \frac{\left|E\left[Y_{f^*}^c\, X_{f_1^*} X_{f_2^*}\right]\right|}{E\left[\left|X_{f_1^*} X_{f_2^*}\right|^2\right] E\left[\left|Y_f^*\right|^2\right]} \qquad (5)$$

The cross-bicoherence measures the phase coherence between resonant wave triads in the two signals. Such phase coupling is required for nonlinear energy exchange. Here the cross-bicoherence is calcualted for the case of two hot wire signals obtained simultaneously at $y^+ = 15$ and $y^+ \approx 200$. Figure 7 shows the resulting $b_{xxy}^2(f_1, f_2)$ which maps to the same f_1^*, f_2^*

domain as shown in Figure 5. The $y^+ = 15$ velocity fluctuation is considered as x(t) and that at $y^+ \approx 200$ as y(t). This figure shows phase coherence among wave triads only within a narrow band contained within the previously described region IIb. These interactions are of all of form $f_1^* - f_2^* = f_1^* - (f_1^* - \delta f^*) = \delta f^*$ where $\delta f^* \approx O(0.5)$. This indicates that there is interaction between wave triads of two comparable and one much lower frequency. This might suggest that there is a phase locking between near wall small scale structure and larger structures of the outer layer. This result, along with the spectral decomposition of skewness presented earlier further underscores the importance of nonlinear mechanisms in characterizing the inner-outer layer interaction.

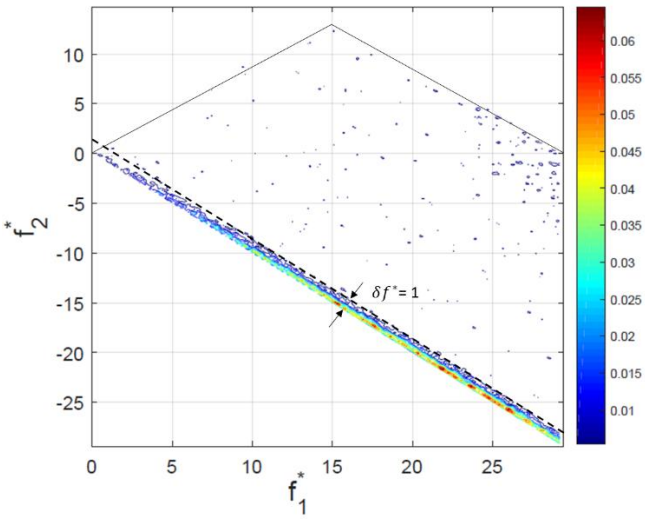

Figure 7. Cross bicoherence of the signal of the location $y^+ = 15$ and $y^+ \approx 200$.

A NONLINEAR SYSTEM MODEL

The polyspectral measurements presented in the previous section underscore the importance of nonlinear mechanisms in the interaction between the logarithmic and near wall regions of the turbulent boundary layer. In order to further characterize this interaction, experiments are performed using a measurement technique in which the nonlinear spetral dynamics characterizing this interaction is captured in terms of a transfer funtion containing both linear and quadratically nonliner system elements. A similar approach has been used in plasma turbulence and in jet transition work (Thomas and Chu 1991). Two hot-wire probes are used for the measurement and their positioning is shown in Figure 9. The first probe is placed at $y^+ = 15$, where primary turbulence peak occurs. The second probe is placed in the log layer ($y^+ \approx 200$) and at the same horizontal location. One serves as the nonlinear system input and the other as the output. The nonlinear system is shown in Figure 10. The objective of the experiment is to determine both the linear and nonlinear system elements for the natural as well as actuated turbulent boundary layer in both drag enhanced and drag suppressed states. Figure 9 also shows the relative position of the probe pair downstream of a flush mounted pulsed-DC actuator for the drag control. The current paper presents the methodology of estimating the transfer functions and quantities derivable from them.

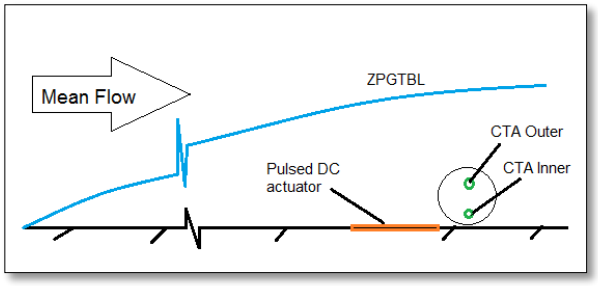

Figure 8: Schematic of the setup.

The schematic of the system model is shown in figure 9.

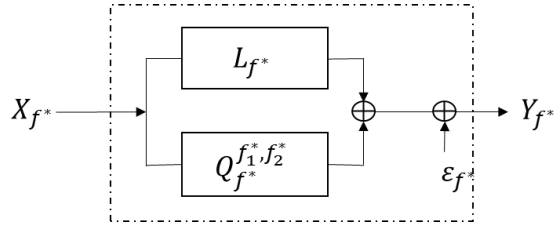

Figure 9: Schematic of the system model.

The input-output relation of the nonlinear system shown in figure 9 can be written as

$$Y_{f^*} = L_{f^*}X_{f^*} + \sum_{\substack{f_1^*, f_2^* \\ f^*=f_1^*+f_2^*}} Q_{f^*}^{f_1^*, f_2^*} X_{f_1^*}X_{f_2^*} + \varepsilon_{f^*} \qquad (6)$$

where L_{f^*} is the linear transfer function, $Q_{f^*}^{f_1^*, f_2^*}$ is the quadratic transfer function and ε_{f^*} is an error term. The error term takes care of all the errors accumulated due to neglect the higher order terms and the inherent noise present in the measurement. By multiplying Eq.6 by X_f^C we can write an expression for linear transfer function

$$L_f = \frac{E[Y_{f^*}X_{f^*}^C] - \sum_{f_1^*, f_2^*} Q_{f^*}^{f_1^*, f_2^*} E[X_{f^*}^C X_{f_1^*}X_{f_2^*}] - E[\varepsilon_{f^*}X_{f^*}^C]}{E[X_{f^*}X_{f^*}^C]} \qquad (7)$$

In a similar fashion the quadratic transfer functions can be computed by multiplying Eq. 6 with $X_{f_1'}^C X_{f_2'}^C$ and taking an ensemble average

$$E\left[Y_{f^*}X_{f_1'}^C X_{f_2'}^C\right] = L_{f^*}E[X_{f^*}X_{f_1'}^C X_{f_2'}^C] + \sum_{f_1^*, f_2^*} Q_{f^*}^{f_1^*, f_2^*} E[X_{f_1^*}X_{f_2^*}X_{f_1'}^C X_{f_2'}^C] + E[\varepsilon_{f^*}X_{f_1'}^C X_{f_2'}^C] \qquad (8)$$

Where $f^* = f_1^* + f_2^* = f_1' + f_2'$

For a Gaussian process the equation (8) and (9) can be further simplified as third order moments are zero for such processes.

$$E[X_{f^*}X_{f_1'}^C X_{f_2'}^C] = 0 \qquad (9)$$

For non-Gaussian processes the third order moments are non-zero and the examples have already been presented in the previous section (cross bispectrum). Equation (8) and (9) can be solved either by matrix method (Kim and Powers, 1988) or by iterative methods. In general the transfer functions can contain a large volume of information. Therefore it is useful to introduce normalized quantities to provide an easier interpretation of input-output relationship. A convenient tool is coherency. It measures the fraction of the power in output signal which can be accounted by the linear and quadratic transfer function model. The total local coherency (Eqn. 10) is defined as sum of local linear coherency, local quadratic coherency, mixed local coherency and error terms and is equal to unity.

$$\gamma_L^2(f^*) + \gamma_Q^2(f^*) + \gamma_{LQ}^2(f^*) + \gamma_n^2(f^*) + < error >= 1 \quad (10)$$

Local linear coherency measures fraction of power in the output signal at frequency f^* due to the linear transfer function.

$$\gamma_L^2(f^*) = \left|L_{f^*}\right|^2 \frac{E[X_{f^*} X_{f^*}^C]}{E[Y_{f^*} Y_{f^*}^C]} \quad (11)$$

Local quadratic coherency measures fraction of power in the output signal at frequency f^* due to the quadratic transfer function.

$$\gamma_Q^2(f^*) = \sum_{f_1^*, f_2^*} \left|Q_{f^*}^{f_1^*, f_2^*}\right|^2 \frac{E[\left|X_{f_1^*} X_{f_2^*}\right|^2]}{E[Y_{f^*} Y_{f^*}^C]} \quad (12)$$

Mixed local coherency measures fraction of output power that results from a non-zero auto bispectrum of input signal. It captures the nonlinear history of the flow at the system input.

$$\gamma_{LQ}^2(f^*) = \frac{2\, Re(L_{f^*} \sum_{f_1^*, f_2^*} \left[Q_k^{f_1^*, f_2^*}\right]^C E[X_{f^*} X_{f_1^*}^C X_{f_2^*}^C])}{E[Y_{f^*} Y_{f^*}^C]} \quad (13)$$

And the error term

$$\gamma_\varepsilon^2(f^*) = \frac{E[\varepsilon_{f^*} \varepsilon_{f^*}^C]}{E[Y_{f^*} Y_{f^*}^C]} \quad (14)$$

Using these metrics the outer layer-inner layer interaction can be quantified for both reduced and enhanced drag conditions and can be compared to the natural flow.

SUMMARY AND CONCLUSIONS

Measurements are presented in a zero pressure gradient turbulent boundary layer at $Re_\tau = 3200$ which are in very good agreement with previous high Reynolds number experiments. Higher order spectra are used to characterize the nonlinear processes involved in the interaction between the near-wall and logarithmic regions. The frequency decomposition of the skewness of near wall fluctuations shows triad interactions between comparable frequencies and a much lower frequency that is characteristic of large-scale outer layer structure. In addition, two-point cross bicoherence measurements show nonlinear phase locking between modes in the near-wall and log regions. This provides motivation for a nonlinear system model of the inner-outer layer interaction. A methodology for obtaining the linear and quadratically nonlinear transfer functions and physical quantities derivable from them is described.

REFERENCES

Adrian, R. J., 2007, Hairpin vortex organization in wall turbulence, Physics of Fluids, 19, 041301.

Canton, J., Orlü, R., Chin, C. and Schlatter, P., 2016, Reynolds number dependence of large scale friction control in turbulent channel flow, Physical Review Fluids, vol.1, no. 8, p.081501.

Ganipathisubramani, B., Hutchins, N., Monty, J. P., Chung, D., and Marusic, I., 2012, Amplitude and frequency modulation in wall turbulence, J. Fluid Mech., Vol. 712, pp. 61-91.

Hutchins, N. and Marusic, I., 2007, Evidence of very long meandering features in the logarithmic region of turbulent boundary layers, J. Fluid Mech., Vol. 579, pp. 1-28.

Kim, K. I. and Powers, E. J., 1988, A digital method of modelling quadratically nonlinear systems with a general random input, IEEE transactions on acoustics, speech and signal processing, vol. 36, no 11

Marusic, I., McKeon, B. J., Monkewitz, P. A., Nagib, H. M., Smits, A. J., & Sreenivasan, K. R., 2010, Wall bounded turbulent flows at high Reynolds number: Recent advances and key issues, Physics of Fluids, Vol. 22, 6, 065103

Monty. J. P., Stewart, J. A., Williams, R. C. and Chong, M. S., 2007, Large scale features in turbulent pipe and channel flows, J. Fluid Mech., 589, p. 147.

Mathis, R., Hutchins, N., and Marusic, I., 2009, large-scale amplitude modulation of the small scale structures in turbulent boundary layers, J. Fluid Mech., Vol. 681, p. 311.

Mathis, R., Marusic, I., Hutchins, N. and Sreenivasan, K. R., 2011, The relationship between the velocity skewness and the amplitude modulation of the small scale by the large scale in turbulent boundary layers, Physics of Fluids, 23, 121702.

Schoppa, W. & Hussain, F. 1998, A large scale control strategy for drag reduction in turbulent boundary layers. Phys. Fluids 10, 1049.

Schoppa, W. & Hussain, F. 2002 Coherent structure generation in near-wall turbulence. J. Fluid Mech. 453, 57–108.

Smits, A. J., McKeon, B. J., and Marusic, I., 2011, High-Reynolds Number Wall Turbulence, Ann. Rev. Fluid Mech., Vol. 43, pp. 353-375.

Thomas, F. O., Corke, T. C., Hussain. F., Duong, A., McGowan, R., Jasinski, C. and Simmons, D., 2016, Turbulent boundary layer drag reduction by active control of streak transient growth, Bulletin of the APS, 69th Annual Meeting of the APS Division of Fluid Dynamics, Vol. 61, no. 20.

Thomas, F. O. and Chu, H. C., 1991, Experimental investigation of the nonlinear spectral dynamics of planar jet transition, Physics of Fluids A, Vol3, p. 1544.